European Polymer Journal 112 (2019) 704–713

Contents lists available at ScienceDirect

European Polymer Journal

journal homepage: www.elsevier.com/locate/europolj

Photopolymerization-assisted self-assembly as a strategy to obtain a dispersion of very high aspect ratio nanostructures in a polystyrene matrix

Ú.M. Montoya Rojo[a], C.C. Riccardi[a], M.D. Ninago[b], A.E. Ciolino[c], M.A. Villar[c], M. Ceolín[d], I.A. Zucchi[a], W.F. Schroeder[a,*]

[a] Institute of Materials Science and Technology (INTEMA), University of Mar del Plata and National Research Council (CONICET), Juan B. Justo 4302, 7600 Mar del Plata, Argentina
[b] Facultad de Ciencias Aplicadas a la Industria, Universidad Nacional de Cuyo (FCAI-UNCUYO), Consejo Nacional de Investigaciones Científicas y Técnicas (CONICET), Bernardo de Irigoyen 375, 5600 San Rafael, Argentina
[c] Planta Piloto de Ingeniería Química, PLAPIQUI (UNS-CONICET), Departamento de Ingeniería Química, Universidad Nacional del Sur, Av. Alem 1253, 8000 Bahía Blanca, Argentina
[d] Instituto de Investigaciones Fisicoquímicas Teóricas y Aplicadas (INIFTA), Universidad Nacional de La Plata, CONICET, CC 16-Suc. 4, 1900 La Plata, Argentina

ARTICLE INFO

Keywords:
Block copolymers
Self-assembly
Photopolymerization

ABSTRACT

Very high aspect ratio nano-objects dispersed in a polymer matrix impart a number of desired characteristics to the material, such as barrier properties to the diffusion of small molecules. Commonly, these dispersions are obtained via top-down procedures that require several time-consuming steps of purification, surface modification, and processing. In this article, we show that it is possible to produce a dispersion of crystalline nano-objects of very high aspect ratio through an *in situ* approach based on photopolymerization-driven self-assembly. For this purpose, a synthesized poly(styrene-*block*-ε-caprolactone) (PS-*b*-PCL) block copolymer was dissolved in styrene (St) monomer, and the solution was slowly photopolymerized at room temperature. Under such conditions, long crystalline nanoribbons dispersed in a PS matrix were obtained after four days of irradiation. The nanostructuration process was investigated by *in situ* small-angle X-ray scattering (SAXS), wide-angle X-ray diffraction (XRD), and transmission electron microscopy (TEM). Obtained results allowed us to conceptualize the formation mechanism of nanoribbons as a stepwise micellization-crystallization-growth process. When photopolymerization at room temperature was replaced by thermal polymerization at 90 °C, a dispersion of amorphous nanorods was obtained. This demonstrated that crystallization of PCL blocks played a dominant role in determining the morphology of the very high aspect ratio nano-objects obtained by photopolymerization.

1. Introduction

Self-assembly of block copolymers (BCP) in polymer matrices has been explored in the last years as an efficient synthetic route for the preparation of nanostructured materials with different morphologies and specific properties [1–3]. The developed morphology depends on several factors, such as length of each block, concentration, thermodynamic compatibility between block-matrix and block-block, and temperature [4,5]. It has been demonstrated that from a suitable selection of initial formulation and self-assembly conditions of the BCP, it is possible to obtain, in a controlled manner, a variety of micellar morphologies (such as spheres, cylinders, vesicles, lamellae) dispersed or organized in the polymer matrix [6–8]. The level of complexity of the self-assembly process increases when one block of the BCP is able to crystallize. While a significant number of papers describing the self-assembly mechanism of semicrystalline BCP in solution have been published in recent years [9–17], the nanostructuration of semicrystalline BCP during polymerization of reactive monomers remains virtually unexplored.

The preparation of nanostructured polymers via initial self-assembly of block copolymers requires that precursors of the polymer matrix act as a block-selective solvent, giving rise to micellar nanostructures before the polymerization reaction. These nanostructures are then fixed by the polymerization reaction of the matrix. Thus, the condition for this approach is that the BCP is self-assembled into micelle structures before the polymerization reaction, and that the miscible block keeps its miscibility during reaction in order to avoid macrophase separation. Under these conditions, the developed morphology depends on a balance of contributions to the free energy, involving the surface energy between the micellar core and the matrix, the stretching of the core-

* Corresponding author.
E-mail address: wschroeder@fi.mdp.edu.ar (W.F. Schroeder).

https://doi.org/10.1016/j.eurpolymj.2018.10.037
Received 30 August 2018; Received in revised form 18 October 2018; Accepted 24 October 2018
Available online 25 October 2018
0014-3057/

forming blocks, and the repulsive interactions between the corona-forming blocks [18].

In the case that the insoluble block is able to crystallize, crystal packing forces play a dominant role in determining the morphology of the nanostructures that are formed [19]. Thin lamellae and elongated structures have been the predominant morphologies observed in these cases. For example, Sinturel et al. [20–22] reported the preparation of nanostructured thermosets by initial self-assembly of a poly(ethylene-*block*-ethylene oxide) block copolymer, PE-*b*-PEO (M_n = 1400 g mol^{-1}; 50 wt% PEO), in unsaturated polyester (UP) resin. In this case, PEO is the miscible block while PE is the crystallizable immiscible block. Initially, a lamellar structure of platelets constituted by a crystallized PE core bordered on both sides by PEO chains was obtained. Curing of the UP resin was performed at 70 °C (below the melting temperature of PE) which allowed to preserve the crystalline structure of the PE core and thus freeze the initially formed nanostructures in the crosslinked network. Zucchi et al. [23] used the same block copolymer than Sinturel et al. [20] dissolved in an epoxy monomer based on diglycidyl ether of bisphenol A (DGEBA). Despite the similar behaviour of the blocks in the epoxy resin (PEO is an epoxy-philic block whereas PE is a crystallizable epoxy-phobic block), the change in the thermoset precursors led to long crystalline nanoribbons dispersed in the epoxy monomer before curing reaction. With the aim of preserving the crystalline structure of these micelles, DGEBA was cured at room temperature by photoinitiated cationic polymerization.

In several examples, the requisite for the initial self-assembly approach is not satisfied, since both blocks of the BCP are initially miscible with the polymer precursors. Under this circumstance, Zheng et al. [3,24] demonstrated that nanostructured polymers can be alternatively obtained through a reaction-induced microphase separation (RIMPS). In this case, although both blocks are initially miscible with the polymer precursors, one of them phase separates during polymerization while the other block remains miscible throughout the reaction. The reduction of the miscibility of the blocks during reaction (one of them to the extreme of the phase separation) is due to a decrease in the entropic contribution to the free energy of mixing as a consequence of the polymerization. On the basis of the RIMPS mechanism, Zheng and co-workers have reported several examples showing the formation of nanostructured epoxy-based thermosets with different BCP, such as poly(ε-caprolactone-*block*-styrene) (PCL-*b*-PS) [25], poly(ε-caprolactone-*block*-*n*-butyl acrylate) (PCL-*b*-PBA) [26], poly(ε-caprolactone-*block*-dimethylsiloxane-*block*-ε-caprolactone) (PCL-*b*-PDMS-*b*-PCL) [27], and poly(styrene-*block*-ε-caprolactone-*block*-*n*-butyl acrylate) (PS-*b*-PCL-*b*-PBA) [28]. In all these examples, the block that became immiscible during reaction was a non-crystalline polymer, and obtained nanostructures were spherical and worm-like micelles, vesicles and lamellae, depending on both concentration and type of BCP used. Meng et al. [29] studied a PEO-*b*-PCL block copolymer dissolved in a stoichiometric solution of DGEBA and 4,4′-diaminodiphenylsulfone (DDS). In this system, PCL was the demixed block during polymerization while PEO kept its miscibility throughout the reaction. Although PCL is a crystallizable block, the reaction was carried out at 150 °C, i.e. above the melting temperature of PCL (around 50 °C). Under such conditions, the core of the formed nanostructures remained amorphous during polymerization, and thus the crystallization did not play a role in the self-assembly process. In this case, spherical micelles with a diameter of 10–20 nm dispersed in the epoxy matrix were obtained. A different situation could occur if the reaction were performed at a temperature lower than the melting temperature of the core-forming block. In such a case, the developed morphology would be governed by a competition between microphase separation, crystallization and polymerization. This situation is explored in the present study.

For this work, an amphiphilic diblock copolymer, PS-*b*-PCL, was synthesized by sequential addition of monomers via living anionic polymerization. The diblock copolymer was dissolved in styrene (St) monomer, which is a good solvent for both blocks before polymerization. Then, nanostructured polymers were obtained by polymerization of St via the RIMPS mechanism, where PCL was the demixed block during reaction. Samples were prepared at two different temperatures of polymerization, 90 and 20 °C, i.e. above and below the melting temperature of the PCL block. Amorphous rod-like micelles dispersed in a PS matrix were obtained at 90 °C, as revealed by transmission electron microscopy (TEM), differential scanning calorimetry (DSC) and wide-angle X-ray diffraction (XRD). On the contrary, a dispersion of long crystalline nanoribbons was obtained at room temperature. Experimental evidence attained from *in situ* time-resolved small-angle X-ray scattering (SAXS) tests allowed us to propose a consistent mechanism for the growth of the ribbon-like micelles during the visible-light photopolymerization at room temperature.

2. Experimental section

2.1. Materials

Styrene monomer (St) was supplied by Aldrich Chemical Co. It was previously purified by distillation to remove most of inhibitor (hydroquinone). Benzoyl peroxide (BPO, Akzo-Nobel) was used as thermal initiator. Camphorquinone (CQ, Aldrich Chem. Co) and ethyl-4-dimethyl aminobenzoate (EDMAB, Aldrich Chem. Co) were used together as a two-component photoinitiating system. A poly(ε-caprolactone) homopolymer (PCL, M_n = 10,000 g/mol, M_w/M_n = 1.40, Aldrich Chemical Co.) was employed to analyze its solubility in polystyrene. Chemical structures of these materials are shown in Fig. 1.

2.2. Synthesis of PS-b-PCL block copolymer

The PS-*b*-PCL block copolymer was synthesized under high vacuum conditions by sequential addition of styrene (Aldrich) and ε-caprolactone (ε-CL, Aldrich) monomers, in a Pyrex® glass reactor equipped with break-seals for the addition of the reagents, and constrictions for removal of products at different stages of reaction. Details on monomer purification, reaction conditions, and design of the apparatus were reported elsewhere [30,31]. Block copolymers were synthesized by using sec-butyllithium (sec-Bu$^-$Li$^+$) as initiator, which was freshly prepared in vacuum from sec-butyl chloride (Fluka) and lithium metal (Fluka). Diphenylethylene (DPE) was purified under vacuum, distilled from calcium hydride and fractionated in glass-sealed ampoules. The addition product between DPE and living poly(styryl) lithium chains was used as initiator for the anionic ring opening polymerization of ε-CL. The reaction between purified DPE and poly(styryl) lithium chains was left to proceed during 3 h, and after that period of time, ε-CL monomer was added. The polymerization was finished after 20 min, by adding degassed acetic acid. The resulting BCP had 38 wt% PCL (calculated from ^{1}H NMR spectrum) and a number average molar mass M_n = 47,000 g/mol (M_w/M_n = 1.02), as determined by gel permeation chromatography (GPC) [30].

2.3. Sample preparation

First, a proper amount of PS-*b*-PCL was blended with St monomer to prepare samples containing 10 wt% BCP. The blend was stirred at room temperature until a homogeneous solution was obtained. Then, the initiator of polymerization was added and the mixture was stirred at room temperature until complete dissolution. The mixture was purged with dry nitrogen at room temperature for 10 min and then, it was transferred to glass capillaries and sealed to avoid the evaporation of St during curing. In the case of thermal curing, BPO in an amount of 2 wt% with respect to C=C groups was added, and the resulting sample was cured in an oil bath at 90 °C. In the case of visible-light photopolymerization at room temperature, a two-component initiating system based on CQ (2 wt%) and EDMAB (2 wt%) was employed, and the sample was irradiated using a ring-shaped array of LEDs, with a

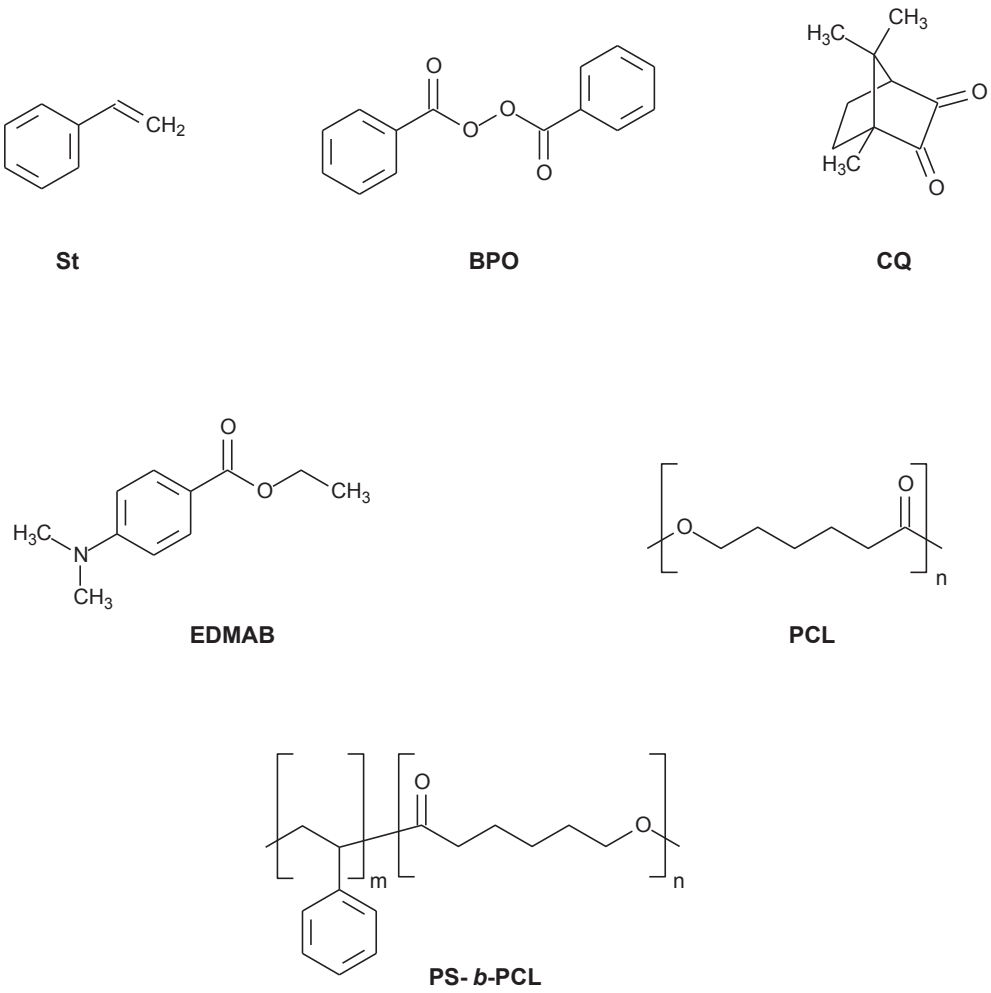

Fig. 1. Chemical structure of used materials.

wavelength range between 410 and 530 nm and an irradiance $I = 140\ \mathrm{mW/cm^2}$. The PS matrices obtained at 90 °C and room temperature presented different molar-mass distributions as shown in the Supplementary Material (Fig. S1).

2.4. Characterization techniques

2.4.1. Differential Scanning Calorimetry (DSC)

Calorimetric measurements were performed on a Perkin-Elmer Pyris 1 differential scanning calorimeter under a dry nitrogen atmosphere. Samples (about 10 mg in weight) were first heated from −50 °C to 150 °C at 10 °C/min (first heating scan), and subsequently cooled to −50 °C at 10 °C/min to detect crystallization (cooling scan). Following the cooling scan, a second heating scan from −50 °C to 150 °C at 10 °C/min was recorded. Glass transition temperature (T_g) was taken as the onset value of the heat capacity change, while the crystallization (T_c) and melting (T_m) temperatures were determined as the maximum and the minimum of both exothermic and endothermic peaks, respectively.

2.4.2. Fourier Transform Infrared Spectroscopy (FTIR)

Through infrared spectroscopy essays it was followed the conversion of vinyl groups as a function of time. Measurements were conducted on a Nicolet 6700 Thermo Scientific device. Spectra were acquired over the range 4000–7000 $\mathrm{cm^{-1}}$ from 32 co-added scans at 4 $\mathrm{cm^{-1}}$ resolution. The sample was placed between two glass windows using a 1.2 mm-rubber spacer. To follow the photopolymerization reaction, the photoactivated mixture was irradiated *in situ* with the ring-shaped array of LEDs and spectra were collected at different exposure times. For the thermal curing reaction, the device was provided with a heated transmission cell (HT-32, Spectra Tech) and a programmable temperature controller (CAL 9500P, Spectra Tech). In both cases, the conversion of vinyl groups was followed by measuring the height of the absorption band at 6134 $\mathrm{cm^{-1}}$, assigned to the $=CH_2$ first overtone.

The evolution of the glass transition temperature of the reacting system as a function of conversion (x) was calculated using Eq. (1) [32], where T_{g0} is the glass transition temperature of the initial reactive mixture, $T_{g\infty}$ is the glass transition temperature of the polymer matrix reacted to full conversion, and $\lambda = \Delta c_{p\infty}/\Delta c_{p0}$, is the ratio of changes in the specific heat through the glass transition for the fully polymerized and the initial samples.

$$(T_g - T_{g0})/(T_{g\infty} - T_{g0}) = \lambda x/[1 - (1 - \lambda)x] \quad (1)$$

2.4.3. Small-Angle X-ray Scattering (SAXS).

SAXS measurements were conducted in a XEUSS 1.0 HR (XENOCS, Grenoble) apparatus equipped with a Pilatus 100 K detector (Dectris, Switzerland) and a microfocus X-ray source (λ = 1.5419 Å). Sample to detector distance was fixed in 1354 mm. The reactive mixture was placed inside a glass capillary (borosilicate) with a thickness of 0.01 mm (Hampton Research) and an external diameter of 1.5 mm. The capillary was placed in a holder mounted in the X-ray beam path so that all the SAXS diagrams were recorded at the same position with an acquisition time of 10 or 20 min for polymerizations at 90 °C or room temperature, respectively. For the photopolymerization experiment, the

LED array was concentrically located to the X-ray beam. The SASfit software package was used to analyze scattering profiles.

2.4.4. Transmission Electron Microscopy (TEM)

TEM images were recorded using a JEOL 100CX electron microscope operated at 100 kV. Ultrathin sections (60 nm in thickness) were obtained at room temperature employing an LKB ultramicrotome equipped with a diamond knife. To increase the contrast, ultrathin sections were stained with RuO_4 vapor prior to TEM examination.

2.4.5. Wide-Angle X-ray Diffraction (XRD)

Wide-angle X-ray diffraction (XRD) data were obtained with an automated X'Pert PRO PANalytical diffractometer. The system is equipped with a graphite monochromator, using Cu Kα (λ = 0.1541 nm) irradiation at 40 kV and 40 mA. Diffraction patterns were recorded in the range of 2θ = 10–40° at the scanning rate and step size of 1.2°/min and 0.02°, respectively.

2.4.6. Transmission optical microscopy (TOM)

TOM was used to determine the phase separation time of PCL homopolymer during polymerization of St. A Leica DMLB microscope equipped with a hot stage (Linkam THMS 600) and a photodetector incorporated in the optical path of the microscope were used for this purpose.

3. Results and discussion

3.1. Miscibility of PCL during the polymerization of St

Before studying the self-assembly characteristics of the BCP (PS-*b*-PCL), it is important to know on the miscibility behaviour of PCL block during St polymerization. For this purpose, a PCL homopolymer with similar molar mass to PCL block in the BCP was selected and used in an equivalent concentration (6.2 wt%) as that present in the blend with 10 wt% BCP. The miscibility of PCL homopolymer in the reactive St solvent was followed by transmission optical microscopy (TOM) during polymerization at two different temperatures: 90 °C and room temperature (20 ± 2 °C). At both temperatures, the blend was initially transparent and exhibited a maximum value of light transmission as shown in the Supplementary Material (Fig. S2). However, a sharp decrease in transmittance was observed after 17 min reaction at 90 °C, and after 15 min reaction at room temperature, due to the phase separation of PCL (see Fig. S2). A set of photographs taken during the polymerization at 90 °C clearly shows the change from transparency to opacity occurred during reaction (Fig. 2).

Based on these results, it can be inferred that although both blocks (PCL and PS) are initially miscible with the St monomer, under the selected conditions PCL block will phase separate during St polymerization resulting in self-assembled structures driven by the mechanism of reaction-induced microphase separation. It should be cleared that the PS block remains miscible with PS matrix during the whole reaction at 90 °C, and up to the vitrification conversion in the photopolymerization at room temperature, as discussed below.

It is important to note that the RIMPS mechanism has been originally developed by S. Zheng and co-workers for nanostructured epoxy networks, which are obtained by step-growth polymerization [3]. In this kind of polymerization, a distribution of condensation species is obtained at any stage of reaction, and the phase behaviour of the system is represented in a pseudo-binary phase diagram corresponding to multicomponent epoxy polymer/BCP mixtures. In contrast, polystyrene matrices are obtained by chain polymerization, where the reaction mixture consists of monomer (St), high-molar-mass polymer (PS), and BCP. Therefore, in the present case, unlike a step-growth polymerization, the phase behaviour during reaction must be represented in a pseudo-ternary phase diagram [33].

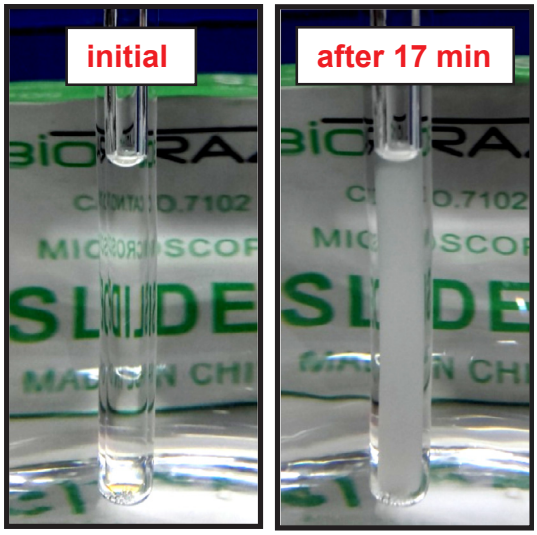

Fig. 2. Photographs taken during the polymerization of St at 90 °C in a blend containing 6.2 wt% PCL homopolymer. Left: initially transparent sample; right: opacity observed after 17 min reaction.

3.2. PCL-b-PS/St blend polymerized at 90 °C

Firstly, we examined the self-assembly behaviour of the BCP during St polymerization at 90 °C with benzoyl peroxide as thermal initiator. The progress of polymerization was monitored by following the decay of an IR absorption band corresponding to the first overtone of vinyl groups at 6134 cm^{-1}. An almost full conversion of vinyl double bonds was achieved after 70 min reaction as shown in Fig. 3. From the conversion-time curve, it can be inferred that micro-phase separation of PCL block occurred at a conversion value around 0.18, based on the time (17 min) at which the transparent to opaque transition for the PCL homopolymer was recorded (Fig. 2).

Fig. 4 shows *in situ* SAXS profiles obtained during polymerization at 90 °C of a sample containing 10 wt% BCP. Measurements were performed in continuous mode, where each SAXS curve resulted from an acquisition time of 10 min. As can be seen, a small change in the scattering profile occurred between 10 and 20 min of reaction, due to the micellization process of the BCP. For polymerization times longer than 20 min, recorded SAXS profiles were almost identical, which shows that the morphology of initially formed nanostructures did not significantly change until the end of the reaction. The sample was

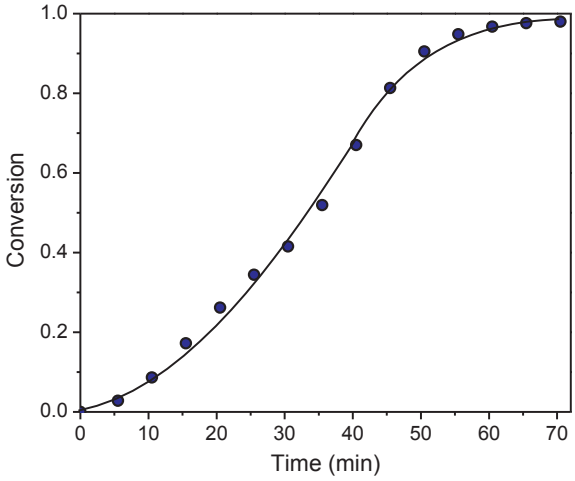

Fig. 3. Conversion of vinyl groups as a function of time for the blend containing 10 wt% BCP, polymerized at 90 °C. The black line is drawn to guide the eye.

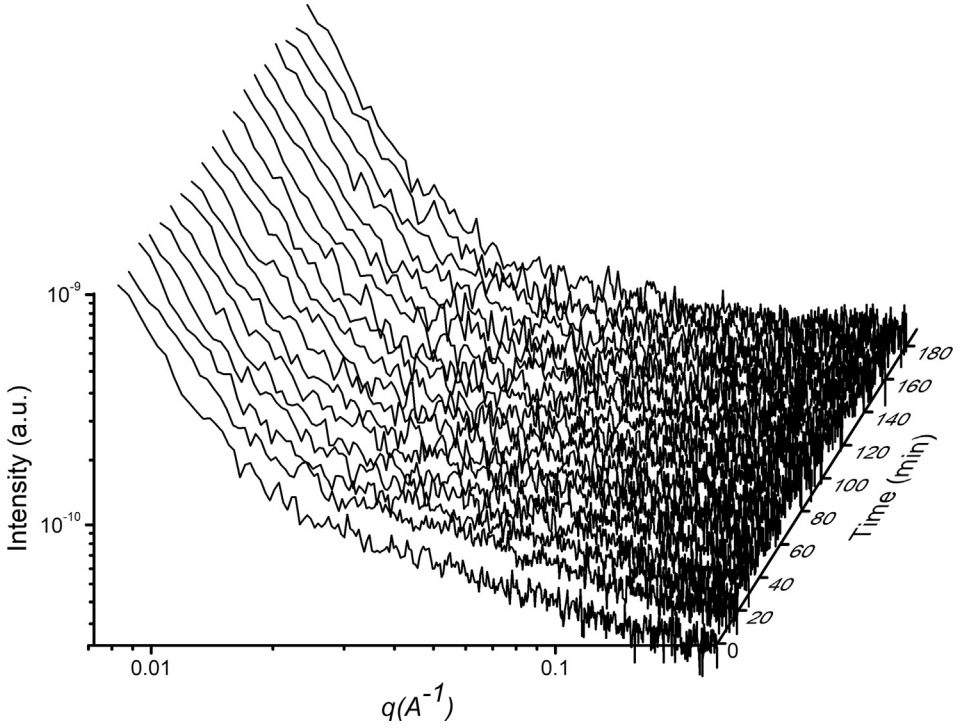

Fig. 4. *In situ* SAXS profiles obtained during polymerization at 90 °C of the sample containing 10 wt% BCP.

visually translucent after the reaction at 90 °C, and maintained the same appearance during the cooling period.

After polymerization at 90 °C, the sample was subjected to DSC tests. As a reference, Fig. 5a and b shows the DSC cooling scan from the melt and the subsequent heating scan for the neat PCL homopolymer and the neat BCP, respectively. During the cooling step, PCL homopolymer displayed a sharp crystallization exotherm at a peak temperature of 27 °C. This is the typical non-isothermal crystallization behaviour of heterogeneously nucleated PCL due to the presence of highly active heterogeneous nuclei in the bulk [34]. DSC subsequent heating scan for the PCL homopolymer showed the melting of the PCL crystals as an endothermic peak at 54 °C.

In the case of the neat BCP (Fig. 5b), several crystallization exotherms were observed during the cooling scan, with distinguishable peaks at 27, −4 and −45 °C. This result is ascribed to a fractionated crystallization phenomenon produced by the confinement of PCL blocks into isolated cylindrical microdomains and by the existence of different nucleation events within such microdomains [35]. Commonly, this phenomenon occurs when the number of microdomains is larger than the number of heterogeneities available to produce nucleation. Therefore, the exotherm at 27 °C is assigned to the crystallization of microdomains containing highly active heterogeneities (those commonly present in bulk PCL), while the exotherm at −4 °C is related to the crystallization of microdomains with less active heterogeneities, which require a higher degree of supercooling. The peak at −45 °C could be assigned to the heterogeneity-free microdomains that crystallized by a homogeneous nucleation process. Note that the homogeneous nucleation should occur at the maximum degree of supercooling just before vitrification (T_g of PCL is approximately −60 °C) [36]. As shown in Fig. 5b, DSC subsequent heating scan presented an endothermic peak at 54 °C due to the melting of PCL crystals, followed by the T_g of PS blocks at 79 °C (onset value).

Fig. 6 shows the DSC cooling scan from the melt and the subsequent heating scan for the sample with 10 wt% BCP polymerized at 90 °C. In

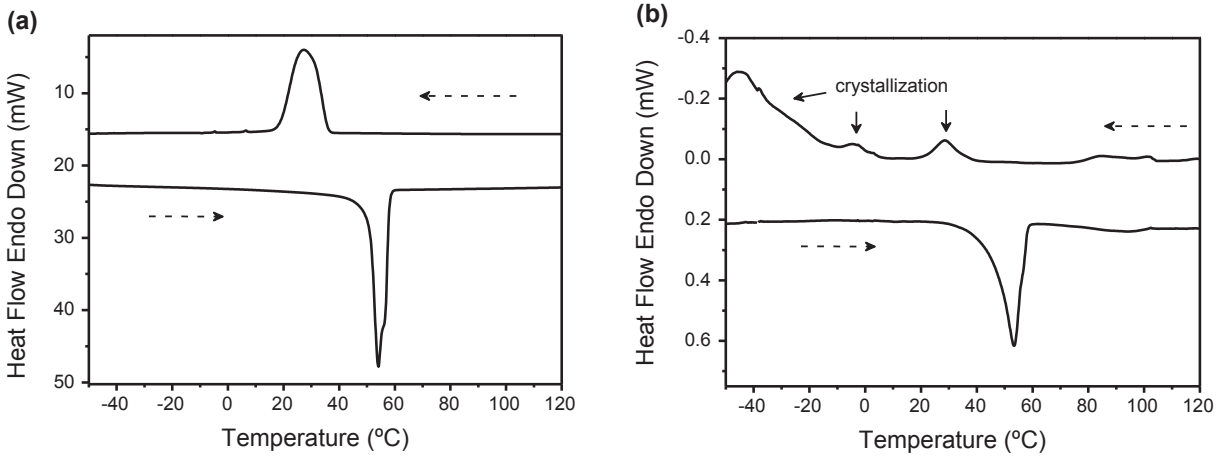

Fig. 5. DSC cooling curves from the melt (above) and subsequent heating scan (below) for: (a) neat PCL homopolymer; (b) neat BCP. In all cases, a rate of 10 °C/min was used.

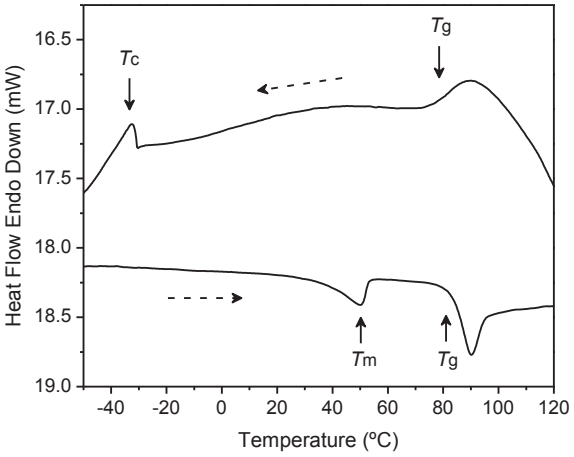

Fig. 6. DSC cooling curve from the melt (above) and subsequent heating scan (below) for a sample containing 10 wt% BCP polymerized at 90 °C. In both runs, a rate of 10 °C/min was used.

this case, a dominant crystallization exotherm can be observed below −35 °C possibly caused by a homogeneous nucleation process of PCL, as previously discussed. The heating step displayed the melting of PCL crystals at a peak temperature of 50 °C, and then the T_g of the PS matrix at 83 °C. This T_g value was significantly lower than that of the bulk PS matrix without BCP (89 °C, see Fig. S3 in the Supplementary Material), which can be attributed to an incomplete demixing of PCL blocks during reaction-induced microphase separation [37]. Based on these results, we can infer that once the reaction ended and the sample was cooled from the polymerization temperature (90 °C) to room temperature, PS matrix vitrified at around 80 °C and crystallization of PCL blocks did not take place.

DSC tests were periodically performed in order to investigate whether confined crystallization of PCL cores occurred during annealing of the sample at room temperature. We did not detect crystallization after four months of annealing, as shown in the Supplementary Material (Fig. S4). These results demonstrated that amorphous-core micelles frozen in a PS matrix were obtained for the sample polymerized at 90 °C.

Fig. 7 shows TEM micrographs at different magnifications of the sample with 10 wt% BCP polymerized at 90 °C. Before the TEM observation, the sample was stained with RuO_4 with the aim of increasing the contrast between the phases. Since PS is preferentially stained by RuO_4 compared to the PCL, PS-rich regions look darker in the TEM images [38]. As can be seen, the micrographs reveal the presence of a population of nanorods dispersed in the PS matrix, with the PS blocks forming the corona of the micelles and the PCL blocks forming the core. Note that coronas look darker than the matrix in the TEM images. This contrast can be ascribed to a higher mass density of PS in the micellar coronas with respect to the matrix. From the analysis of these and other images, we calculated that the contour length of these micelles ranged from 30 to 220 nm, and the width from 12 to 25 nm.

It has been documented that the morphology adopted by micelles prepared from crystalline-coil BCP in reactive solvents depends on a competition between two self-organizing mechanisms: microphase separation and crystallization [39]. When the polymerization reaction is performed above the melting temperature of the crystallizable core-forming block, and the resulting T_g of the matrix is higher than the crystallization temperature, vitrification of the matrix occurs before the crystallization of the micellar core in the cooling process. Under this circumstance, the morphology of the nanostructure generated at high temperature is preserved and is not affected by the crystallization of the core-forming block. This was the case of the sample with 10 wt% BCP polymerized at 90 °C, where crystallization was not detected within the experimental time used herein.

A different situation occurs when the reaction is performed at a temperature below the melting temperature of the core-forming block. In this case, if the insoluble block is able to crystallize during the polymerization reaction, crystal packing forces play a dominant role in determining the morphology of the nanostructures that are formed. We analyze this case in the following section.

3.3. PS-b-PCL/St blend photopolymerized at room temperature

For these experiments, we used a protocol of slow photopolymerization of St at room temperature, i.e. below the melting temperature of the PCL block. The initiating mechanism has been discussed in the literature and is briefly described here [40]. Visible-light irradiation produces the excitation of CQ to its singlet, which rapidly undergoes intersystem crossing to the triplet state. The excited triplet is reduced by EDMAB to give rise to ketyl and α-amino free radicals. The amino radical initiates the bulk polymerization of St while the ketyl radical is not an efficient initiator and dimerizes.

The progress of the photopolymerization of St was monitored by FTIR spectroscopy. Blue[1] dots in Fig. 8 represent the conversion of vinyl groups of St as a function of irradiation time, while black points indicate the evolution of the glass transition temperature of the matrix with the conversion degree as predicted by Eq. (1), where $\lambda = 0.158$, $T_{g0} = -30$ °C and $T_{g\infty} = 62$ °C. As can be seen, a vitrification conversion of 0.88 was reached after four days of irradiation. From the conversion-time curve, we can infer that micro-phase separation of PCL blocks took place at a conversion value of approximately 0.12, based on the time at which the transparent to opaque transition was observed (15 min).

To investigate the nanostructuration process of the BCP during photopolymerization of St, in-situ SAXS experiments were performed. Scattering profiles were collected every 1 h during 96 h of reaction, with an acquisition time of 20 min. The temporal evolution of SAXS curves is shown in Fig. 9. As can be seen, there were no significant changes in the scattering profile during the first 40 h of irradiation. In addition, the collected curves during this time period were almost identical to those obtained after 20 min of reaction at 90 °C (see Fig. S5 in the Supplementary Material), suggesting the existence of nanorods during this stage. Suddenly, a pronounced change in the SAXS profile took place between 41 and 44 h of irradiation, as depicted in Fig. 9. During this time, a strong increase of scattering intensity was recorded, along with the incipient development of a set of correlation peaks with the characteristic sequence of a lamellar arrangement of planar nano-objects, as demonstrated below. From 44 h to the end of the test (96 h), no major changes in SAXS curves were observed, except for a small increase in the scattering intensity at the low-q region, consistent with a micellar elongation process. The sample was visually opaque after 96 h of irradiation.

Once finished the in-situ SAXS test, the sample was subjected to XRD measurements to detect whether crystallization of PCL blocks took place during photopolymerization of St. The recorded diffraction pattern is compared with that obtained before the photopolymerization process in Fig. 10. For interpretation purposes, the XRD pattern corresponding to the neat PCL homopolymer is also included. As can be seen, the photopolymerized sample exhibited a large amorphous halo centred at $2\theta = 20^\circ$ due to the PS matrix, and two diffraction peaks at $2\theta = 22.4$ and 24.6° corresponding to the (1 1 0) and (2 0 0) planes of the normal orthorhombic crystal structure of PCL [41]. These results show that core-forming PCL blocks crystallized during the photopolymerization of St in the same crystalline structure as commonly observed in bulk PCL. In addition, the photopolymerized sample was analyzed by DSC. The first heating scan displayed the T_g of the PS matrix at 22 °C (onset value) followed immediately by the melting of

[1] For interpretation of color in Figs. 8 and 11, the reader is referred to the web version of this article.

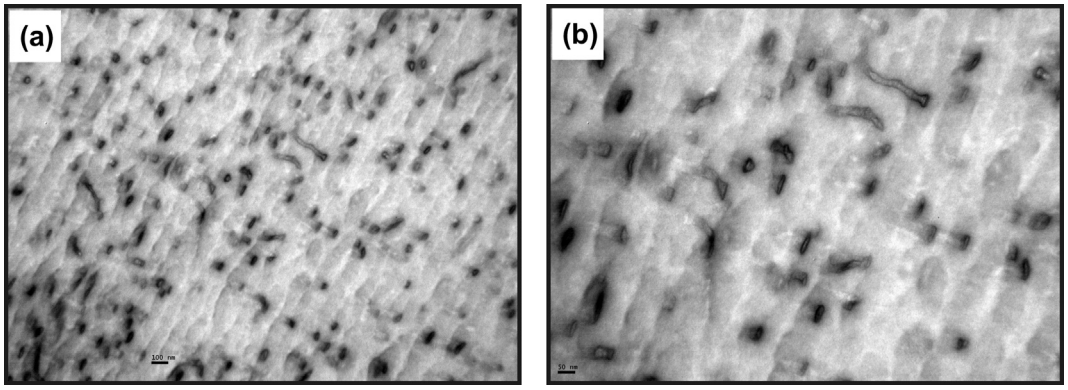

Fig. 7. TEM images of the sample with 10 wt% BCP polymerized at 90 °C. The specimen was stained with RuO_4 vapor prior to the TEM observation. (a) Lower magnification, the black bar represents 100 nm; and (b) higher magnification, the black bar represents 50 nm.

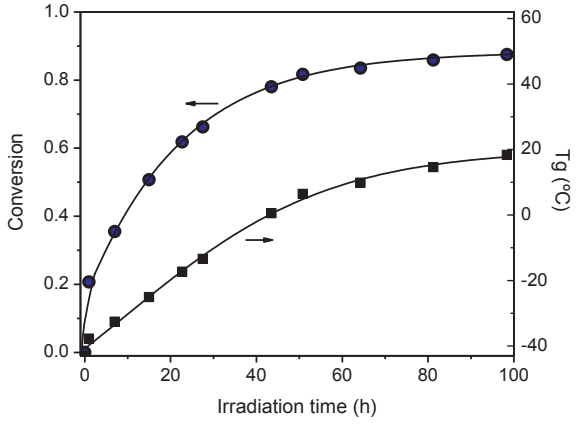

Fig. 8. Conversion of St and evolution of T_g of the matrix as a function of irradiation time for the mixture containing 10 wt% BCP, photopolymerized at room temperature. Irradiation was conducted with a LED unit operating in the visible region of the spectrum (410–530 nm, 140 mW/cm^2). Black lines were drawn to guide the eye.

PCL crystals at a peak temperature of 52 °C (see Fig. S6 in the Supplementary Material). On the basis of these results, it is possible to infer that the marked change in the SAXS profiles between 41 and 44 h of irradiation, assigned to a transition from nanorods to lamellar nanoparticles, was promoted by the crystallization of PCL blocks. This assertion is supported by the fact that crystalline-core micelles commonly exhibit planar structures with lamellar arrangement [19]. Note that at 41 h of irradiation, the T_g of the matrix was approximately 0 °C (see Fig. 8), which is below the crystallization temperature (20 °C). Under these conditions, the crystallization of PCL blocks took place before the vitrification of the PS matrix, unlike the sample polymerized at 90 °C.

Fig. 11 shows TEM images at different magnifications of the sample with 10 wt% BCP photopolymerized at room temperature. Elongated micelles with lengths ranging from 300 nm to more than 2 μm, coexisting with much shorter micelles of about 60 nm in length, can be observed. It is also noted that elongated micelles tend to orient parallel to each other, resulting in face-to-face stacking into lamellar arrangements. This feature evidences the planar nature of these structures, which can be described as ribbon-like micelles. A magnified image of one of these lamellar arrangements is shown in Fig. 11b. Here, it is observed a stack of micelles viewed edge-on with crystallized PCL blocks forming the core (lighter line) sandwiched by two coronal PS layers (darker lines). From this image, it can be estimated that the thickness of these micelles is around 15 nm and the average lamellar period is about 40 nm.

Further information on these nanostructures was obtained by analyzing the SAXS profile recorded after photopolymerization at room temperature (Fig. 12). The magnitude of the slope in the low-q region (Guinier regime) was equal to 2.2, which indicates the presence of planar nano-objects [42]. As stated above, the scattering profile displays a principal maximum of spatial correlation at $q^* = 0.14\,\mathrm{nm}^{-1}$, and a secondary maximum located at $2q^*$. Such a sequence corresponds with a lamellar arrangement featuring an average distance between nano-objects of 44.9 nm ($2\pi/q^*$), which is in accordance with the lamellar period estimated from the TEM image. As can be noted in Fig. 9, the correlation maxima were not clearly evident between 44 and 96 h of irradiation; however, they developed progressively with the annealing time after photopolymerization. This can be ascribed to an increase of the electron density contrast due to the densification of the crystalline phase [41,43]. It should be pointed out that the SAXS profile shown in Fig. 12 was acquired one week after the photopolymerization process was completed. The SAXS curve was analyzed using the SASfit software package. The form factor was modeled with the *HomogeneousXS* algorithm, assuming the simultaneous contribution of long planar objects (length $L > 1$ μm and thickness $h = 5$ nm) and shorter planar objects ($L = 60$ nm and $h = 5$ nm), as revealed by TEM images. Keep in mind that the thickness of long objects is the same as that of short objects. In order to account for the maxima observed in the SAXS profile, a lamellar structure factor (*Paracrystalline* model) was added, with an average stacking separation of 40 nm. As can be noted, the optimized fitting parameters are in very good agreement with the structural features obtained by TEM image analysis. With these parameters, an excellent fitting of the SAXS curve was achieved (Fig. 12).

Obtained results lead us to conceptualize the formation of these nanostructures as a three-step self-assembly process. Initially, both blocks of the BCP were soluble in the St monomer, however microphase separation occurred at early stages of the photopolymerization process as a result of the demixing of PCL blocks produced by the increase in St conversion. In this first step, rod-like micelles with an amorphous-core were developed. Here, the morphology was governed by the block copolymer characteristics (composition, size, and relative proportion of the blocks), and the nature of the reactive solvent. The second step took place after almost two days irradiation at room temperature, where a morphological transformation, from nanorods to short planar nano-objects (platelets), was produced. This flattening of the micelles was driven by the packing forces involved during the crystallization of the core-forming PCL blocks, resulting in platelets of around 5 nm in thickness surrounded on both sides by PS blocks. Note that if the polymerization kinetics had not been slow enough, vitrification of the matrix could have occurred before the micellar crystallization, resulting in rod-like micelles frozen in the PS matrix, similar to the sample polymerized at 90 °C. The last step consisted in a micellar elongation process that took place during the time elapsed between the crystallization and the vitrification of the matrix. We believe that this

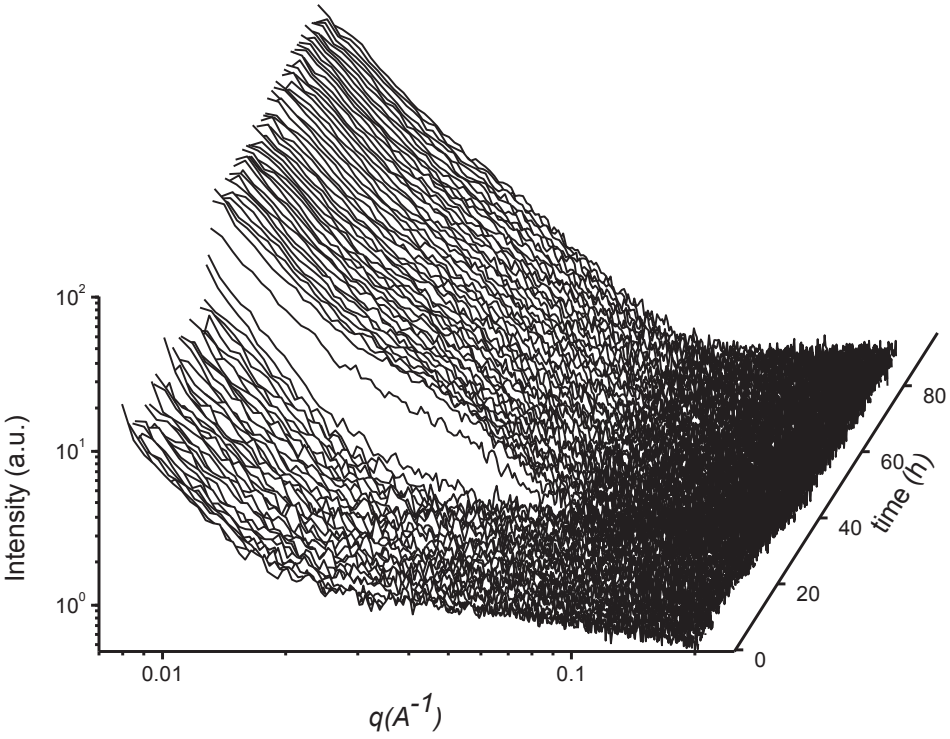

Fig. 9. *In situ* SAXS profiles obtained during photopolymerization at room temperature of the sample containing 10 wt% BCP. Irradiation was conducted with a LED unit operating in the visible region of the spectrum (410–530 nm, 140 mW/cm^2).

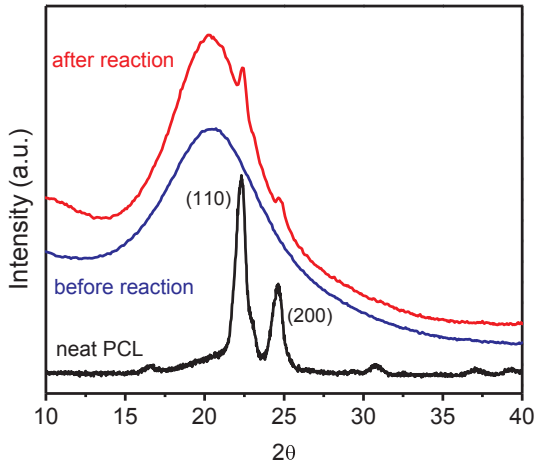

Fig. 10. XRD profiles recorded before and after photopolymerization reaction at room temperature. The profile corresponding to the neat PCL homopolymer is also included for comparison purposes.

process of micellar growth occurred through an end-to-end coupling of the crystalline platelets. There are three reasons for such a speculation. First, the thickness of the long ribbon-like micelles is the same as that of the platelets, as revealed by TEM and SAXS. Second, the growth by end-to-end coupling requires that the ends of two planar micelles collide in such an orientation that their crystal planes match at the interface [44]. Close inspection of TEM images reveals the presence of individual platelets that are aligned but not connected, such as those pointed by the red arrow in Fig. 11b. This phenomenon is probably due to the mismatch of the crystal planes at the interface between both micelles. On the other hand, TEM images show that most of the uncoupled residual platelets are oriented perpendicular to the growth directions of the elongated micelles, which would explain why these platelets could not be aggregated.

It has been demonstrated that the growth by end-to-end coupling of crystalline micelles follows the same growth kinetics as a condensation polymerization [44]. Therefore, the length of the micelles should increase linearly with growth time. In the present study, the growth time (the third step) could be easily manipulated by adjusting photonic parameters, such as the light power used to drive the photopolymerization process. We believe that this strategy could be used as a versatile way to control the length of the micelles that are formed. Work is in progress in this direction.

As can be seen in Fig. 11, morphologies generated by photopolymerization at room temperature could be compared to those observed in dispersions of intercalated/exfoliated nanoclays in polymer matrices. It is well known that clay nanosheets of very large aspect ratio impart some desired characteristics to the polymer matrix, such as barrier properties to the diffusion of small molecules [45]. However, clay-polymer nanocomposites are commonly prepared via top-down procedures that require several time-consuming steps of purification, surface modification, and processing [45]. The approach presented in this work could offer the possibility of generating materials with improved barrier properties through a more versatile and simpler bottom-up route.

4. Conclusions

Slow photopolymerization at room temperature of a blend consisting of 10 wt% PS-*b*-PCL dissolved in St monomer led to a population of long crystalline nanoribbons dispersed in a PS matrix. The formation of these nanostructures was conceptualized as a three-step self-assembly process. Initially, both blocks of the BCP were soluble in St, although micro-phase separation occurred at early stages of the photopolymerization process as a result of the demixing of PCL blocks. Consequently, rod-like micelles with an amorphous PCL core were firstly formed. After almost two days of irradiation, a morphological transformation from nanorods to platelets took place, which was driven by the crystallization of core-forming PCL blocks. Finally, micellar growth by end-to-end coupling of crystalline platelets was produced. A

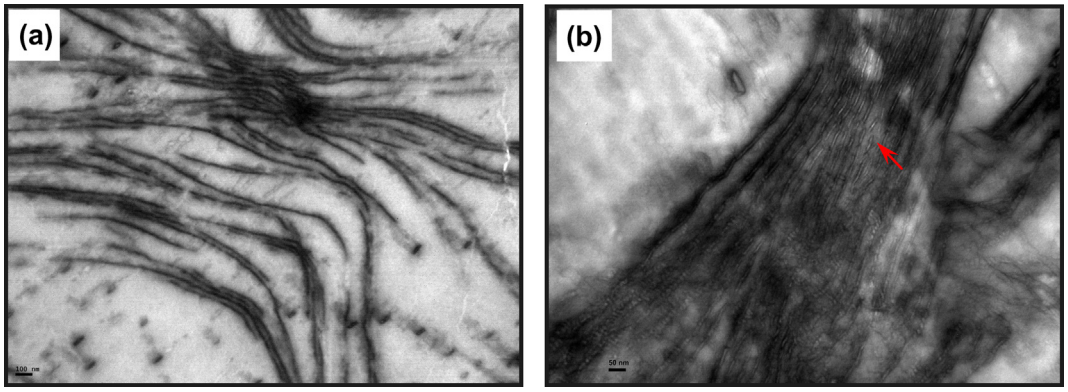

Fig. 11. TEM images of a sample with 10 wt% BCP photopolymerized during 96 h at room temperature. The specimen was stained with RuO_4 vapor prior to the TEM observation. (a) Lower magnification, the black bar represents 100 nm; and (b) higher magnification, the black bar represents 50 nm.

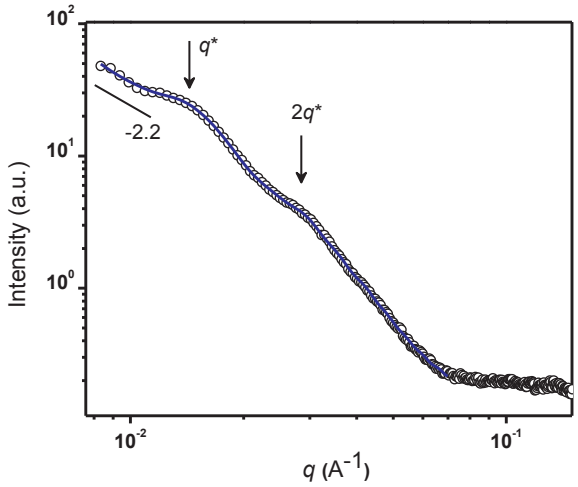

Fig. 12. SAXS profile of the sample with 10 wt% BCP photopolymerized during 96 h at room temperature. The blue line represents the data modeling assuming a population of long and short planar objects, with a lamellar structure factor. (For interpretation of the references to color in this figure legend, the reader is referred to the web version of this article.)

different situation occurred when the polymerization reaction was carried out at 90 °C, i.e. above the melting temperature of PCL. In this case, the crystallization of PCL blocks was prevented by the vitrification of the matrix during the cooling process. Under these conditions, a dispersion of nanorods with amorphous core was obtained. These results demonstrated that crystallization of core-forming PCL blocks played a dominant role in determining the morphology of the nanostructures obtained by photopolymerization at room temperature. Very high aspect ratio nanoribbons could impart some desired characteristics to the polymer matrix, such as barrier properties for packaging applications.

5. Data availability

The raw/processed data required to reproduce these findings cannot be shared at this time due to time limitations.

Acknowledgements

The financial support of the following institutions is gratefully acknowledged: National Research Council (CONICET, Argentina), National Agency for the Promotion of Science and Technology (ANPCyT, Argentina), and University of Mar del Plata. C.C.R., M.D.N., A.E.C., M.A.V., M.C., I.A.Z. and W.F.S. are staff members of CONICET, Argentina.

Author contributions

The manuscript was written through contributions of all authors. All authors have given approval to the final version of the manuscript.

Appendix A. Supplementary material

Size exclusion chromatography (SEC) analysis of PS matrices synthesized at 90 °C and room temperature; optical transmittance of PCL/St blend during photopolymerization at room temperature; DSC heating scan for the bulk PS matrix without BCP, polymerized at 90 °C; DSC heating scan for a sample containing 10 wt% BCP polymerized at 90 °C and annealed for four months at room temperature; comparison of the SAXS profile obtained after 24 h of irradiation at room temperature with that obtained after 1 h of reaction at 90 °C, for samples containing 10 wt% BCP; DSC heating scan of the photopolymerized sample containing 10 wt% BCP. Supplementary data to this article can be found online at https://doi.org/10.1016/j.eurpolymj.2018.10.037.

References

[1] L. Ruiz-Pérez, G.J. Royston, J.P.A. Fairclough, A.J. Ryan, Toughening by nanostructure, Polymer 49 (2008) 4475–4488, https://doi.org/10.1016/j.polymer.2008.07.048.
[2] T.J. Hermel-Davidock, H.S. Tang, D.J. Murray, S.F. Hahn, Control of the block copolymer morphology in templated epoxy thermosets, J. Polym. Sci. Part B Polym. Phys. 45 (2007) 3338–3348, https://doi.org/10.1002/polb.21336.
[3] S. Zheng, Nanostructured epoxies by the use of block copolymers, in: J.P. Pascault, R.J.J. Williams (Eds.), Epoxy Polym. New Mater. Innov. Wiley-Blackwell, 2010, pp. 79–108.
[4] J. Bang, U. Jeong, D.Y. Ryu, T.P. Russell, C.J. Hawker, Block copolymer nanolithography: translation of molecular level control to nanoscale patterns, Adv. Mater. 21 (2009) 4769–4792, https://doi.org/10.1002/adma.200803302.
[5] J. Wu, Y.S. Thio, F.S. Bates, Structure and properties of PBO–PEO diblock copolymer modified epoxy, J. Polym. Sci. Part B Polym. Phys. 43 (2005) 1950–1965, https://doi.org/10.1002/polb.20488.
[6] H.E. Romeo, I.A. Zucchi, M. Rico, C.E. Hoppe, R.J.J. Williams, From spherical micelles to hexagonally packed cylinders: the cure cycle determines nanostructures generated in block copolymer/epoxy blends, Macromolecules 46 (2013) 4854–4861, https://doi.org/10.1021/ma400778s.
[7] J. Puig, I.A. Zucchi, M. Ceolín, W.F. Schroeder, R.J.J. Williams, Evolution of morphologies of a PE-b-PEO block copolymer in an epoxy solvent induced by polymerization followed by crystallization-driven self-assembly of PE blocks during cooling, RSC Adv. 6 (2016) 34903–34912, https://doi.org/10.1039/C6RA03019J.
[8] J. Puig, M. Ceolín, R.J.J. Williams, W.F. Schroeder, I.A. Zucchi, Controlling the generation of bilayer and multilayer vesicles in block copolymer/epoxy blends by a slow photopolymerization process, Soft Matter. 13 (2017) 7341–7351, https://doi.org/10.1039/C7SM01660C.
[9] L. Yin, T.P. Lodge, M.A. Hillmyer, A. Stepwise, Micellization–crystallization route to oblate ellipsoidal, cylindrical, and bilayer micelles with polyethylene cores in water, Macromolecules 45 (2012) 9460–9467, https://doi.org/10.1021/ma302069s.
[10] L. Shen, H. Wang, G. Guerin, C. Wu, I. Manners, M.A. Winnik, A Micellar sphere-to-cylinder transition of poly(ferrocenyldimethylsilane-b-2-vinylpyridine) in a

selective solvent driven by crystallization, Macromolecules 41 (2008) 4380–4389, https://doi.org/10.1021/ma702852j.
[11] X. Wang, G. Guerin, H. Wang, Y. Wang, I. Manners, M.A. Winnik, Cylindrical block copolymer micelles and co-micelles of controlled length and architecture, Science 317 (2007) 644–647, https://doi.org/10.1126/science.1141382.
[12] E.L. Kynaston, O.E.C. Gould, J. Gwyther, G.R. Whittell, M.A. Winnik, I. Manners, Fiber-like micelles from the crystallization-driven self-assembly of poly(3-heptylselenophene)-block-polystyrene, Macromol. Chem. Phys. 216 (2015) 685–695, https://doi.org/10.1002/macp.201400541.
[13] H. Qiu, Y. Gao, V.A. Du, R. Harniman, M.A. Winnik, I. Manners, Branched micelles by living crystallization-driven block copolymer self-assembly under kinetic control, J. Am. Chem. Soc. 137 (2015) 2375–2385, https://doi.org/10.1021/ja5126808.
[14] H. Qiu, Z.M. Hudson, M.A. Winnik, I. Manners, Multidimensional hierarchical self-assembly of amphiphilic cylindrical block comicelles, Science 347 (2015) 1329–1332, https://doi.org/10.1126/science.1261816.
[15] Y. Gao, H. Qiu, H. Zhou, X. Li, R. Harniman, M.A. Winnik, I. Manners, Crystallization-driven solution self-assembly of block copolymers with a photocleavable junction, J. Am. Chem. Soc. 137 (2015) 2203–2206, https://doi.org/10.1021/ja512968b.
[16] N. McGrath, F.H. Schacher, H. Qiu, S. Mann, M.A. Winnik, I. Manners, Synthesis and crystallization-driven solution self-assembly of polyferrocenylsilane diblock copolymers with polymethacrylate corona-forming blocks, Polym. Chem. 5 (2014) 1923–1929, https://doi.org/10.1039/C3PY01383A.
[17] J. Xu, H. Zhou, Q. Yu, I. Manners, M.A. Winnik, Competitive self-assembly kinetics as a route to control the morphology of core-crystalline cylindrical micelles, J. Am. Chem. Soc. 140 (2018) 2619–2628, https://doi.org/10.1021/jacs.7b12444.
[18] A. Choucair, A. Eisenberg, Control of amphiphilic block copolymer morphologies using solution conditions, Eur. Phys. J. E 10 (2003) 37–44, https://doi.org/10.1140/epje/e2003-00002-5.
[19] J.J. Crassous, P. Schurtenberger, M. Ballauff, A.M. Mihut, Design of block copolymer micelles via crystallization, Polymer 62 (2015) A1–A13, https://doi.org/10.1016/j.polymer.2015.02.030.
[20] C. Sinturel, M. Vayer, R. Erre, H. Amenitsch, Thermal induced mobility of self-assembled platelets of polyethylene-block-poly(ethylene oxide) in liquid precursors of unsaturated polyester thermoset, Eur. Polym. J. 45 (2009) 2505–2512, https://doi.org/10.1016/j.eurpolymj.2009.06.001.
[21] C. Sinturel, M. Vayer, R. Erre, H. Amenitsch, Nanostructured polymers obtained from polyethylene-block-poly(ethylene oxide) block copolymer in unsaturated polyester, Macromolecules 40 (2007) 2532–2538, https://doi.org/10.1021/ma062849r.
[22] R.N. Mahaling, M. Vayer, S. Guillot, C. Sinturel, Oriented array of polyethylene-block-poly(ethylene oxide) nanoplatelets in unsaturated polyesters cross-linked coatings, Eur. Polym. J. 47 (2011) 2277–2282, https://doi.org/10.1016/j.eurpolymj.2011.10.001.
[23] I.A. Zucchi, W.F. Schroeder, Nanoribbons with semicrystalline core dispersed in a visible-light photopolymerized epoxy network, Polymer 56 (2015) 300–308, https://doi.org/10.1016/j.polymer.2014.11.053.
[24] F. Meng, S. Zheng, H. Li, Q. Liang, T. Liu, Formation of ordered nanostructures in epoxy thermosets: a mechanism of reaction-induced microphase separation, Macromolecules 39 (2006) 5072–5080, https://doi.org/10.1021/ma060004+.
[25] R. Yu, S. Zheng, X. Li, J. Wang, Reaction-induced microphase separation in epoxy thermosets containing block copolymers composed of polystyrene and poly(ε-caprolactone): influence of copolymer architectures on formation of nanophases, Macromolecules 45 (2012) 9155–9168, https://doi.org/10.1021/ma3017212.
[26] Z. Xu, S. Zheng, Reaction-induced microphase separation in epoxy thermosets containing poly(ε-caprolactone)-block-poly(n-butyl acrylate) diblock copolymer, Macromolecules 40 (2007) 2548–2558, https://doi.org/10.1021/ma062486v.
[27] Z. Xu, S. Zheng, Morphology and thermomechanical properties of nanostructured thermosetting blends of epoxy resin and poly(ε-caprolactone)-block-poly-dimethylsiloxane-block-poly(ε-caprolactone) triblock copolymer, Polymer 48 (2007) 6134–6144, https://doi.org/10.1016/j.polymer.2007.07.072.
[28] W. Fan, L. Wang, S. Zheng, Double reaction-induced microphase separation in epoxy resin containing polystyrene-block-poly(ε-caprolactone)-block-poly(n-butyl acrylate) ABC triblock copolymer, Macromolecules 43 (2010) 10600–10611, https://doi.org/10.1021/ma101945f.
[29] F. Meng, S. Zheng, T. Liu, Epoxy resin containing poly(ethylene oxide)-block-poly(ε-caprolactone) diblock copolymer: effect of curing agents on nanostructures, Polymer 47 (2006) 7590–7600, https://doi.org/10.1016/j.polymer.2006.08.050.
[30] D. Uhrig, J.W. Mays, Experimental techniques in high-vacuum anionic polymerization, J. Polym. Sci. Part A Polym. Chem. 43 (2005) 6179–6222, https://doi.org/10.1002/pola.21016.
[31] N. Hadjichristidis, H. Iatrou, S. Pispas, M. Pitsikalis, Anionic polymerization: high vacuum techniques, J. Polym. Sci. Part A Polym. Chem. 38 (2000) 3211–3234, https://doi.org/10.1002/1099-0518(20000915)38:18<3211::AID-POLA10>3.0.CO;2-L.
[32] J.P. Pascault, R.J.J. Williams, Glass transition temperature versus conversion relationships for thermosetting polymers, J. Polym. Sci. Part B Polym. Phys. 28 (1990) 85–95, https://doi.org/10.1002/polb.1990.090280107.
[33] W.F. Schroeder, M.I. Aranguren, G.E. Eliçabe, J. Borrajo, Free-radical polymerization induced macrophase separation in poly(methyl methacrylate)/dimethacrylate blends: experiment and modeling, Eur. Polym. J. 49 (2013) 3956–3965, https://doi.org/10.1016/j.eurpolymj.2013.08.027.
[34] R.A. Pérez, M.E. Córdova, J.V. López, J.N. Hoskins, B. Zhang, S.M. Grayson, A.J. Müller, Nucleation, crystallization, self-nucleation and thermal fractionation of cyclic and linear poly(ε-caprolactone)s, React. Funct. Polym. 80 (2014) 71–82, https://doi.org/10.1016/j.reactfunctpolym.2013.10.013.
[35] R.M. Michell, A.J. Müller, Confined crystallization of polymeric materials, Prog. Polym. Sci. 54–55 (2016) 183–213, https://doi.org/10.1016/j.progpolymsci.2015.10.007.
[36] S. Tiptipakorn, N. Keungputpong, S. Phothiphiphit, S. Rimdusit, Effects of polycaprolactone molecular weights on thermal and mechanical properties of polybenzoxazine, J. Appl. Polym. Sci. 132 (2015), https://doi.org/10.1002/app.41915.
[37] V. Balsamo, F. von Gyldenfeldt, R. Stadler, Thermal behavior and spherulitic superstructures of SBC triblock copolymers based on polystyrene (S), polybutadiene (B) and a crystallizable poly(ε-caprolactone) (C) block, Macromol. Chem. Phys. 197 (1996) 3317–3341, https://doi.org/10.1002/macp.1996.021971021.
[38] J.S. Trent, J.I. Scheinbeim, P.R. Couchman, Ruthenium tetraoxide staining of polymers for electron microscopy, Macromolecules 16 (1983) 589–598, https://doi.org/10.1021/ma00238a021.
[39] W.-N. He, J.-T. Xu, Crystallization assisted self-assembly of semicrystalline block copolymers, Prog. Polym. Sci. 37 (2012) 1350–1400, https://doi.org/10.1016/j.progpolymsci.2012.05.002.
[40] I.E. dell'Erba, F.D. Martínez, C.E. Hoppe, G.E. Eliçabe, M. Ceolín, I.A. Zucchi, W.F. Schroeder, Mechanism of particle formation in silver/epoxy nanocomposites obtained through a visible-light-assisted in situ synthesis, Langmuir (2017), https://doi.org/10.1021/acs.langmuir.7b01936.
[41] Y. Zhang, H. Huo, J. Li, Y. Shang, Y. Chen, S.S. Funari, S. Jiang, Crystallization behavior of poly(ε-caprolactone) and poly (ε-caprolactone)/LiClO4 complexes from the melt, CrystEngComm 14 (2012) 7972–7980, https://doi.org/10.1039/C2CE25126D.
[42] M. Nakano, K. Matsumoto, H. Matsuoka, H. Yamaoka, Characterization of micellization behavior of amphiphilic polymer having octadecyl group by small-angle X-ray and neutron scattering, Macromolecules 32 (1999) 4023–4029, https://doi.org/10.1021/ma981675d.
[43] B.L. Caetano, F. Meneau, C.V. Santilli, S.H. Pulcinelli, M. Magnani, V. Briois, Mechanisms of SnO2 nanoparticles formation and growth in acid ethanol solution derived from SAXS and combined Raman–XAS time-resolved studies, Chem. Mater. 26 (2014) 6777–6785, https://doi.org/10.1021/cm5032688.
[44] W.-N. He, B. Zhou, J.-T. Xu, B.-Y. Du, Z.-Q. Fan, Two growth modes of semicrystalline cylindrical poly(ε-caprolactone)-b-poly(ethylene oxide) micelles, Macromolecules 45 (2012) 9768–9778, https://doi.org/10.1021/ma301267k.
[45] M. Alexandre, P. Dubois, Polymer-layered silicate nanocomposites: preparation, properties and uses of a new class of materials, Mater. Sci. Eng. R Rep. 28 (2000) 1–63, https://doi.org/10.1016/S0927-796X(00)00012-7.